Article

Heat Transfer Coefficient of a Building: A Constant with Limited Variability or Dynamically Variable?

Ljubomir Jankovic *, Grant Henshaw, Christopher Tsang, Xinyi Zhang, Richard Fitton and William Swan

Energy House Labs, University of Salford, Manchester M5 4WT, UK; g.p.henshaw@salford.ac.uk (G.H.);
c.tsang1@salford.ac.uk (C.T.); x.zhang15@edu.salford.ac.uk (X.Z.); r.fitton@salford.ac.uk (R.F.);
w.c.swan@salford.ac.uk (W.S.)
* Correspondence: l.jankovic@salford.ac.uk; Tel.: +44-7932-176-444

Abstract: The heat transfer coefficient, or the HTC, is an industry-standard indicator of building energy performance. It is predicated on an assumption that it is of a constant value, and several different methods have been developed to measure and calculate the HTC as a constant. Whilst there are limited variations in the results obtained from these different methods, none of these methods consider a possibility that the HTC could be dynamically variable. Our experimental work shows that the HTC is not a constant. The experimental evidence based on our environmental chambers, which contain detached houses and in which the ambient air temperature can be controlled between −24 °C and +51 °C, with additional relative humidity control and with weather rigs that can introduce solar radiation, rain, and snow, shows that the HTC is dynamically variable. The analysis of data from the fully instrumented and monitored houses in combination with calibrated simulation models and data processing scripts based on genetic algorithm optimization provide experimental evidence of the dynamic variability of the HTC. This research increases the understanding of buildings physics properties and has the potential to change the way the heat transfer coefficient is used in building performance analysis.

Keywords: heat transfer coefficient (HTC); thermal diffusivity; time constant; energy performance; dynamic variability; experimental evidence; building physics; environmental chambers; genetic algorithm; machine learning; simulation models

1. Introduction

The heat transfer coefficient (HTC) is an industry-standard indicator of building energy performance. International Standard ISO 13789 [1] defines the heat loss coefficient as the "*Sum of transmission and ventilation heat loss coefficient*", where transmission heat loss coefficient is defined as "*Heat flow rate from the heated space to the external environment by transmission divided by the temperature difference between internal and external environments*" and ventilation heat loss coefficient is defined as "*Heat flow rate from the heated space to the external environment by ventilation divided by the temperature difference between internal and external environments*".

Whilst the above definition provides the scope for dynamic variability, a widely adopted approach in industry is that the HTC is a constant, and several methods have been developed to measure it and calculate it as a constant. Although there are limited variations in the results from these methods, none of them consider the possibility that the HTC could be dynamically variable.

Our experimental work shows that the HTC is not a constant. We conducted experiments in the Environmental Chamber of Energy House 2.0, with one of the two detached houses, where we controlled the ambient air temperature between −24 °C and +51 °C, relative humidity, and introduced weather conditions like solar radiation, rain, and snow. These experiments provided evidence of the HTC s dynamic variability.

Analysis of data from a fully instrumented and monitored house, combined with calibrated simulation models and data processing scripts based on genetic algorithm optimization, provides evidence that supports the dynamic variability of the HTC.

Why does the HTC variability matter? Fitton and co-authors [2] defined the performance gap as follows:

$$\text{Performance gap} = \frac{\text{actual consumption} - \text{theoretical consumption}}{\text{theoretical consumption}} \times 100 \qquad (1)$$

The actual consumption can only be established when the building performance is measured after construction. At that stage, the performance gap cannot be easily reduced, potentially leading to the significant underperformance of buildings. It is therefore of paramount importance to determine theoretical consumption at the design stage as accurately as possible and thus reduce the performance gap before construction. Considering that theoretical consumption is a function of the HTC and considering that the HTC is deemed to be constant, the HTC variability will create significant uncertainties in establishing and reducing the performance gap.

1.1. The Current State of the Research Field

In his doctoral thesis, Eastwood [3] investigated the HTC variability in dwellings influenced by the boundary conditions, including the measurement accuracy of indoor air temperature, outdoor air temperature, internal heat gains, wind speed, infiltration, and ventilation heat loss, party-wall heat transfer, ground-floor heat transfer, losses to adjacent dwellings or unoccupied spaces, and estimates of solar gains. The work aimed to improve the accuracy of measuring the thermal performance of dwellings. Out of circa 30 dwellings measured, the HTC variation was between 202.5 W/K and 208.8 W/K for in-use HTC and between 197.5 W/K and 199.9 W/K for co-heating HTC. This variability is therefore attributed to measurement errors rather than to the variability of the HTC itself.

A limited variability of the HTC has been attributed to different measurement methods, such as in-use HTC versus a co-heating HTC, as well as to the circumstances during the tests and instrumentation accuracy [4].

Sougkakis and co-authors [5] studied the suitability of a quick U-value of buildings (QUB) method to create consistent and robust estimates of the HTC. In 147 tests of a detached house at the University of Nottingham, they found that over 95% of the results were within ±15% from the mean value. In other words, the intention was to demonstrate consistency with a constant value.

In a similar study of the QUB method, Ahmad and co-workers [6] found that a simulation of QUB experiments during the winter months were within ±15% of the steady state HTC.

Juric and co-authors studied the Sereine method [7], a dynamic in situ test method for determining a dwelling s heat transfer coefficient (HTC) and transmission heat transfer rate (HTR). It applies a pseudo-random heating pattern to an unoccupied house, using external temperature and heating power as inputs to an RC model selected via the Bayesian information criterion. The method controls solar gains, seals ventilation, and accounts for external conditions through an equivalent temperature approach. Validation includes a field study at the French National Solar Energy Institute, where the results aligned with a co-heating test within uncertainty limits and EnergyPlus simulations across

21 French locations, showing seasonal variations and higher uncertainty for externally insulated buildings. The test duration range was from 24 to 96 h, with a recommended minimum of 24–72 h depending on the archetype and climate.

Vighio and co-authors [8] worked on experimental measurement and theoretical validation of an Overall Thermal Transfer Value or OTTV in W/m^2, using an Eco-Home Case Study Building. They recorded daily fluctuations in the OTTV, approximately between −30 W/m^2 and +180 W/m^2, for 30 days in September 2023. They also developed an OTTV equation and found a strong linear correlation between the equation-generated values and values generated by the EQUEST simulation engine. The authors home country Malaysia, together with Pakistan, Sri Lanka, Hong Kong, Thailand, and Singapore, have incorporated the OTTV in their building regulations. Although the OTTV is different from the HTC, both are indicators of building energy performance, where the OTTV is a variable, and the HTC is deemed to be constant.

Industry stakeholders recognize the challenge of accurately characterizing building performance, though commercial sensitivity limits the available literature on in-use heat transfer coefficient (HTC) measurement methods. The SMETER TEST project provides the most comprehensive comparison of commercial methodologies, evaluating eight SMETER technologies in a 30-home UK field trial [9]. Among these, Build Test Solutions Smart HTC underwent validation against co-heating tests, showing <1% deviation and <4% repeatability variation over a minimum 21-day monitoring period [10]. Some industry methods, such as HomeLink s "Time to Lose 1 °C" (TTL) [11], measure related heat loss characteristics rather than the HTC directly.

1.2. Measuring and Modelling the HTC

Fitton [2] reported significant variations in the HTC measurements carried out using the same experimental setups. Twelve methods have been developed to measure the HTC, including the co-heating test, quick U-value of buildings (QUB), ISABELE, PSTAR/STEM, and others, where all of these methods measure the HTC as a constant, with typical expected errors between 3% and 30% [2].

The HTC of domestic buildings is commonly measured using the co-heating (aggregate heat loss) test method [12,13]. This test involves heating the internal spaces of an unoccupied building to an elevated, stable temperature (typically around 21 °C), while measuring the electrical heat input required to maintain this temperature over a set period (typically two to three weeks). By plotting the daily heat input against the internal and external temperature difference (ΔT), the total heat loss (fabric and infiltration) can be quantified. Marshall et al. applied co-heating tests under controlled conditions, demonstrating precise HTC measurements and emphasizing the value of controlled testing to accurately assess building fabric performance [14]. Farmer et al. also used co-heating tests to quantify incremental improvements in the HTC through staged retrofits of a solid-wall Victorian dwelling, highlighting the effectiveness of the method for evaluating thermal impacts of retrofit interventions [15]. Additionally, Jack et al. validated the reliability of co-heating tests by demonstrating consistency (±10%) in the HTC measurements across multiple independent tests, confirming the robustness of this method [16].

The HTC predictions can also be modeled using steady-state methods such as the Standard Assessment Procedure (SAP), or dynamic thermal simulation (DTS) tools like DesignBuilder [17,18]. SAP employs a bottom-up approach, aggregating fabric and infiltration heat loss, whereas DTS tools simulate aggregate heat loss dynamically at hourly intervals. Johnston et al. presented empirical data from 38 co-heating tests conducted on 25 distinct dwellings, all complying with the UK s Building Regulations Part L1A 2006. The authors utilized these co-heating tests to obtain measured HTC,

providing valuable insights into the fabric performance of dwellings built to contemporary regulatory standards [19]. Parker et al. demonstrated the value of calibrating DTS models against the HTC data from co-heating tests in retrofitted solid-wall dwellings, significantly improving model accuracy and enhancing retrofit decision making [20].

Fitton et al. evaluated rapid commercial methods for measuring the HTC against the traditional co-heating test [21]. Saint-Gobain s QUB [5,22] and the Veritherm method [23] both performed dynamic HTC measurements of unoccupied dwellings over a single night, considerably shorter than the duration typically required for co-heating tests. Both methods involve a dynamic protocol comprising an initial stabilization period at constant internal temperature, followed by a heating period with constant power input, and ending with a free cooling phase. Each method relies on assumptions about the fabric performance to estimate the required power input, and both utilize integrated hardware and software to control internal conditions, measure power input, and analyze the collected data. A key difference in equipment between the methods is that Veritherm uses air circulation fans during testing, whereas the QUBs does not. The results show that when measurement uncertainty is considered, HTC values from these alternative methods generally align with those obtained from the co-heating test. However, Veritherm s measurement uncertainty is up to twice that of the QUBs. Additionally, the HTC measurements from QUB are approximately 15% lower than those from the co-heating test, whereas the Veritherm results are about 6% lower. The results are summarized in Table 1 [21].

Table 1. HTC measured using three different methods (source: [21]).

HTC Measurement Method	HTC Value (W/K)	Difference from Co-Heating (%)
Co-heating	76.7 ± 2.1	
QUB	65.1 ± 5.6	−15
Veritherm	71.9	−6

1.3. The Knowledge Gap

Whilst the above is by no means an exhaustive account of the state of the research field, a clear knowledge gap is beginning to emerge. The HTC is generally deemed to be constant, with limited variability due to specific test conditions and measurement uncertainties, as corroborated by the results in Table 1. It also appears that the HTC has always been calculated from carefully planned test data. In the remainder of this paper, we will explain how the HTC relates to the fundamental physics properties of materials and will introduce experimental evidence of its variability that is well beyond the measurement discrepancies and uncertainties. We will also demonstrate how the HTC can be reverse-engineered from data from an ongoing monitoring of a building, without any preconditioning or other preparations of the building.

2. Materials and Methods

2.1. Linking the HTC to Dynamic Heat Transfer in a Building

In this section, we will establish the link between the HTC and the fundamental physics properties of a building.

The overall heat loss from a building is calculated as follows [24]:

$$Q = HTC \times (T_i - T_o) \tag{2}$$

where

Q—overall heat loss rate (W);

HTC—heat transfer coefficient (W/K);
T_i—internal air temperature (K);
T_o—external air temperature (K).

The heat transfer coefficient consists of the following components:

$$HTC = H_c + H_{tb} + H_v \tag{3}$$

where

H_c—conductive heat loss coefficient (W/K);
H_{tb}—thermal bridging heat loss coefficient (W/K);
H_v—ventilation and infiltration heat loss coefficient (W/K).

Each of the components of the HTC is defined further below. The fabric heat loss coefficient [25] is defined as follows:

$$H_c = \sum_{i=1}^{i=n} U_i A_i \tag{4}$$

where

H_c—fabric heat loss coefficient (W/K);
U_i—thermal transmittance of the i-th building element (W/(m²K));
A_i—surface area of the i-th building element (m²);
n—number of building elements.

The thermal bridging heat loss coefficient is defined as follows:

$$H_{tb} = \sum_{i=1}^{i=N} L_i \Psi_i \tag{5}$$

where

H_{tb}—thermal bridging heat loss coefficient (W/K);
L_i—length of the i-th linear thermal bridge (m);
Ψ_i—linear thermal transmittance of the i-th thermal bridge (W/(m·K)).

Equation (5) represents the linear thermal bridging only, occurring at junctions between building elements. Point thermal bridging, which occurs when a thermally conductive element penetrates an insulation layer, is considered in the U-value calculations.

The ventilation and infiltration heat loss coefficient is defined as follows:

$$H_v = \frac{N \times V \times c \times \rho}{3600} \tag{6}$$

where

H_v—ventilation and infiltration heat loss coefficient (W/K);
N—volume air change per hour (h⁻¹);
V—building volume (m³);
c—specific heat of air (J/(kg·K));
ϱ—density of air (kg/m³);
3600—seconds in an hour.

The only building material property is in Equation (4), contained in the transmittance of the wall (the U-value), and is thermal conductivity:

$$R = \frac{d}{k} \tag{7}$$

where

d—wall thickness in meters (m);

k—thermal conductivity in W/(m·K).

For a multilayered wall, the resistance of all layers are added together to obtain the total resistance:

$$\sum R = R_i + R_1 + R_2 + R_3 + R_4 + R_o \tag{8}$$

where

R_i—internal surface resistance;

R_o—external surface resistance;

R_1, R_2, R_3…—resistances of individual construction layers;

and where R_i and R_o account for convective and radiative components.

The thermal transmittance (the U-value) is then calculated as the inverse of the sum of thermal resistances for each individual building component:

$$U = \frac{1}{\sum R} \tag{9}$$

U-values for surface areas with point thermal bridges could be either calculated separately, and used with the corresponding surface areas in Equation (4), or alternatively, modelling tools such as DesignBuilder [18] have the functionality for U-value calculation with integrated point thermal bridges.

Thermal conductivity is the only physics property in Equations (2)–(6). As thermal conductivity does not change, Equations (2)–(6) represent steady-state building heat transfer.

However, the heat diffusion equation developed by Fourier [26,27] uses thermal diffusivity for dynamic heat transfer, instead of a single physics parameter for steady state heat transfer:

$$\nabla^2 T + \frac{\dot{q}}{k} = \frac{1}{\alpha} \times \frac{\partial T}{\partial t} \tag{10}$$

where

T—temperature (K);

$\dot{q}$—heat flux (W/m^2);

k—thermal conductivity in W/(m·K);

α—thermal diffusivity (m^2/s);

t—time (s);

and where thermal diffusivity is defined as follows:

$$\alpha = \frac{k}{\rho c} \tag{11}$$

where

k—thermal conductivity in W/(m·K);

ρ—density (kg/m^3);

c—specific heat (J/(kg·K)).

The representation of building heat transfer using thermal diffusivity, with three physics properties of materials (conductivity, density, and specific heat), corresponds much closer to the dynamic processes in buildings, instead of using a steady state approach with a single physics property of materials (conductivity) in Equations (2)–(6). But how can thermal diffusivity be used to represent heat transfer of a specific building?

This is explained using the approach developed on the basis of a simplified heat balance equation [24]:

$$C \times \frac{dT_{room}}{dt} = -Q_{loss} + Q_{sol} + Q_{int} \qquad (12)$$

where

C—effective thermal capacitance in MJ/K;

Q_{loss}–heat gain from solar radiation (W);

Q_{sol}–heat gain from solar radiation (W);

Q_{int}—internal heat gain in the building arising from heating or from casual gains (W).

Equation (12) can be rearranged as follows:

$$\frac{dT_{room}}{dt} + \frac{HTC}{C} \times T_{room} = \frac{HTC}{C} \times T_{amb} + \frac{Q_{sol} + Q_{int}}{C} \qquad (13)$$

where

T_{room}—difference between room temperature and the initial room temperature $T_r - T_{r,0}$;

T_{amb}–difference between ambient air temperature and the initial room temperature $T_a - T_{r,0}$.

The solution of differential equation (13) can be expressed as follows:

$$T_{room} = (T_{amb} + \frac{Q_{int}+Q_{sol}}{HTC}) \times (1 - e^{-\frac{t \times HTC}{C}}) \qquad (14)$$

This can be rewritten as follows:

$$T_{room} = (T_{amb} + \frac{Q_{int} + Q_{sol}}{HTC}) \times (1 - e^{-\frac{t}{tc}}) \qquad (15)$$

where time constant is defined as follows:

$$tc = \frac{C}{HTC} \qquad (16)$$

The time constant represents the time it takes to go through 63% of the change from an initial event, such as heating on time, to the final equilibrium state. The effective thermal capacitance is the following:

$$C = m \times c = V \times \rho \times c \qquad (17)$$

where

m—mass (kg);

V—volume (m³);

c—specific heat (J/(kg·K)).

As the HTC is proportional to thermal conductivity k (HTC $\propto$ B k) where B is the proportionality constant, the time constant can be expressed as follows:

$$tc = \frac{V \times \rho \times c}{B \times k} = \frac{1}{\alpha \times z} \qquad (18)$$

where

α—thermal diffusivity (m²/s);

z—proportionality constant that represents the relationship B/V.

Equation (15) can now be rewritten as follows:

$$T_{room} = (T_{amb} + \frac{Q_{int} + Q_{sol}}{HTC}) \times (1 - e^{-t \times \alpha \times z}) \qquad (19)$$

This links thermal diffusivity α with a simple dynamic temperature equation for a building.

Therefore, whilst Equations (2)–(9) represent steady-state heat transfer, the HTC variability can only be established under dynamic heat transfer, as per Equations (10)–

(19). Dynamic heat transfer will therefore be the focus of our analysis in the remainder of this article.

It is important to point out that the HTC accounts for all thermal exchanges between the building and its surroundings, including contributions from ground interactions, unheated spaces, differently conditioned zones where applicable, and sky vault interactions.

The material introduced in this section will facilitate our experimental investigation in the Experiments and results section.

2.2. The Test Facility

This research was carried out under controlled conditions in the Energy House 2.0 (Figure 1), and it used experimental data from eHome2 (Figure 2) by Saint-Gobain and Barratt Developments, constructed inside Environmental Chamber 1 in Energy House 2.0.

Figure 1. Energy House 2.0 research facility at the University of Salford.

Figure 2. eHome2 inside Environmental Chamber 1 in Energy House 2.0.

Energy House 2.0 is a globally unique building-performance test facility. Constructed to allow for the full-scale testing of structures under a controlled range of climatic conditions, the facility comprises two large chambers, capable of accommodating four family homes, two in each chamber. These chambers feature soil-filled pits, 1200 mm deep, isolated from the ground beneath and surrounding the pit by insulation. The walls and ceilings of each chamber are also insulated, providing isolation from the external climate and ensuring high levels of airtightness.

Each chamber is independently conditioned by a large heating, ventilation, and air conditioning (HVAC) system. Additionally, weather rigs are deployed to provide further climatic effects. These rigs control the climate within the chambers by manipulating various factors, such as temperature, humidity, wind speed and others, as follows:

- Temperature: (−24 °C to +51 °C);
- Relative Humidity (20% to 90%);
- Wind (up to ~17 m/s);
- Rain (up to 200 mm/h);
- Solar Radiation (up to 1200 W/m²);
- Snow (up to 250 mm per day).

Temperature and relative humidity can be held at a constant steady state or varied in seasonal or daily patterns.

2.3. The Test Building—eHome2

eHome2, by Saint-Gobain and Barratt Developments (Figure 2), is a 3-bedroom detached home built using closed panel timber-frame construction, insulated with mineral wool. It is clad externally with a proprietary brick slip system and render [21]. The house has an insulated concrete floor structure, double glazed windows and patio doors, and a roof insulated with 400 mm of mineral wool insulation. The house is heated by a Valliant air source heat pump, which also supplies domestic hot water.

eHome2 constructions, adapted from an earlier data set [28], are specified in Table 2 and calculated U-values are shown in Table 3. The overall window U-value with frame was calculated as 1.2 W/(m²K).

Table 2. eHome2 constructions (adapted from [28]).

Layer	Material	Thickness (mm)	Conductivity (W/mK)	Thermal Resistance (m²K/W)
Brick external wall				
External finish	Weberwall brick slip finishing system	15	0.72	0.021
External board	BG glassroc x	12.5	0.1865	0.067
Cavity	Ventilated cavity	25	-	0.71
Sheathing	Oriented Strand Board	9	0.13	0.069
Outer Insulation	TFR35 Insulation, 8.8% bridging with flange ($\lambda = 0.13$)	47	0.035	0.947
Core insulation	TFR35 Insulation, 1.7% bridging with flange ($\lambda = 0.13$)	151	0.035	3.831
Inner insulation	TFR35 Insulation, 8.8% bridging with flange ($\lambda = 0.13$)	47	0.035	0.947
Additional sheathing	Oriented Strand Board	9	0.13	0.069
Service void	Service void with 8.8% bridging with wooden battens ($\lambda = 0.13$)	35	-	0.518
Internal Finish	Gyproc Wallboard	15	0.19	0.079
Rendered external wall				
External finish	Webersill TF finish coat and Weberend LCA rapid base coat	7.5	0.72	0.0104
External board	BG glassroc x	12.5	0.1865	0.067
Cavity	Ventilated cavity	25	-	0.71
Sheathing	Oriented Strand Board	9	0.13	0.069
Outer Insulation	TFR35 Insulation, 8.8% bridging with flange ($\lambda = 0.13$)	47	0.035	0.947
Core insulation	TFR35 Insulation, 1.7% bridging with flange ($\lambda = 0.13$)	151	0.035	3.831
Inner insulation	TFR35 Insulation, 8.8% bridging with flange ($\lambda = 0.13$)	47	0.035	0.947
Additional sheathing	Oriented Strand Board	9	0.13	0.069
Service void	Service void with 8.8% bridging with wooden battens ($\lambda = 0.13$)	35	-	0.518
Internal Finish	Gyproc Wallboard	15	0.19	0.079
Loft ceiling				
Primary insulation	Isover Spacesaver roof insulation	300	0.044	6.818
Secondary insulation	Isover Spacesaver roof insulation, 9% bridging with wooden batons ($\lambda = 0.13$)	100	0.044	2.092
Ceiling	Gyproc Wallboard	15	0.19	0.079
Pitched roof construction				
External	Concrete tiles (roofing)	10	1.5	0.007
Ventilation	Air gap	10	-	0.15
Underlayment	Roofing Felt	5	0.19	0.026
Internal partitions				
Surface 1	Gypsum plasterboard	15	0.19	0.079
Air space	Air gap	100	-	0.15
Surface 2	Gypsum plasterboard	15	0.19	0.079
Internal floor construction				
Floor surface	Caberdek chipboard floor	22	0.13	0.169
Sheathing	Oriented Strand Board	15	0.13	0.115
Air space	Air gap 254 mm	254	-	0.230
Ceiling	Gyproc wallboard	15	0.19	0.079
Ground floor construction				
Floor construction	450 mm NUG375 + 75 mm Screed	450	0.058	7.759
External door construction				
Door	Painted Oak	35	0.19	0.184

Table 3. Calculated U-values of eHome2 (Source [28]).

Building Component	U-Value (W/m²K)
Brick external wall U-value	0.13
Rendered external wall U-value	0.13
Loft ceiling U-value	0.11
Ground floor U-value	0.11
Windows U-value	1.20
French Door U-value	/
External Door U-value	1.20
Internal partition U-value	1.89
Internal floor U-value (W/m²K)	1.16
Internal door U-value (W/m²K)	2.82

2.4. Simulation Models

A simulation model of eHome2 was initially created in DesignBuilder [18] (Figure 3) and exported into EnergyPlus [29] in order to enable the creation of a custom schedule for dynamic heating and cooling, with details in Figure 4.

Figure 3. Model of eHome2 in DesignBuilder.

```
Schedule:Compact,
    DynamicTest,              !- Name
    Any Number,               !- Schedule Type Limits Name
    Through: 1/1,             !- Field 1
    For: AllDays,             !- Field 2
    Until: 24:00,             !- Field 3
    5,                        !- Field 4
    Through: 1/7,             !- Field 5
```

```
For: AllDays,              !- Field 6
Until: 24:00,              !- Field 7
50,                        !- Field 8
Through: 12/31,            !- Field 9
For: AllDays,              !- Field 10
Until: 24:00,              !- Field 11
5;                         !- Field 12
```

Figure 4. Dynamic heating and cooling schedule in EnergyPlus.

The meaning of the schedule in Figure 4 is that the building internal air temperature is kept at 5 °C, over the first 24 h of the simulation, where 1/1 denotes month/day, and then for the next seven days, until day 7 of month 1 the target temperature is set to 50 °C, and after that it is set back to 5 °C again for the rest of the simulation year. The text after the exclamation symbol on every line represent comments.

The environmental parameters monitored in the Chamber at one-minute time interval were the following: air temperature at 36 points; relative humidity at 36 points; and sub-soil temperature under the center of each house. Chamber sensor locations are shown in Figure 5.

× HygroVUE 10
(temperature and humidity)
× HygroVUE 10 with radiation
sealed on the facade
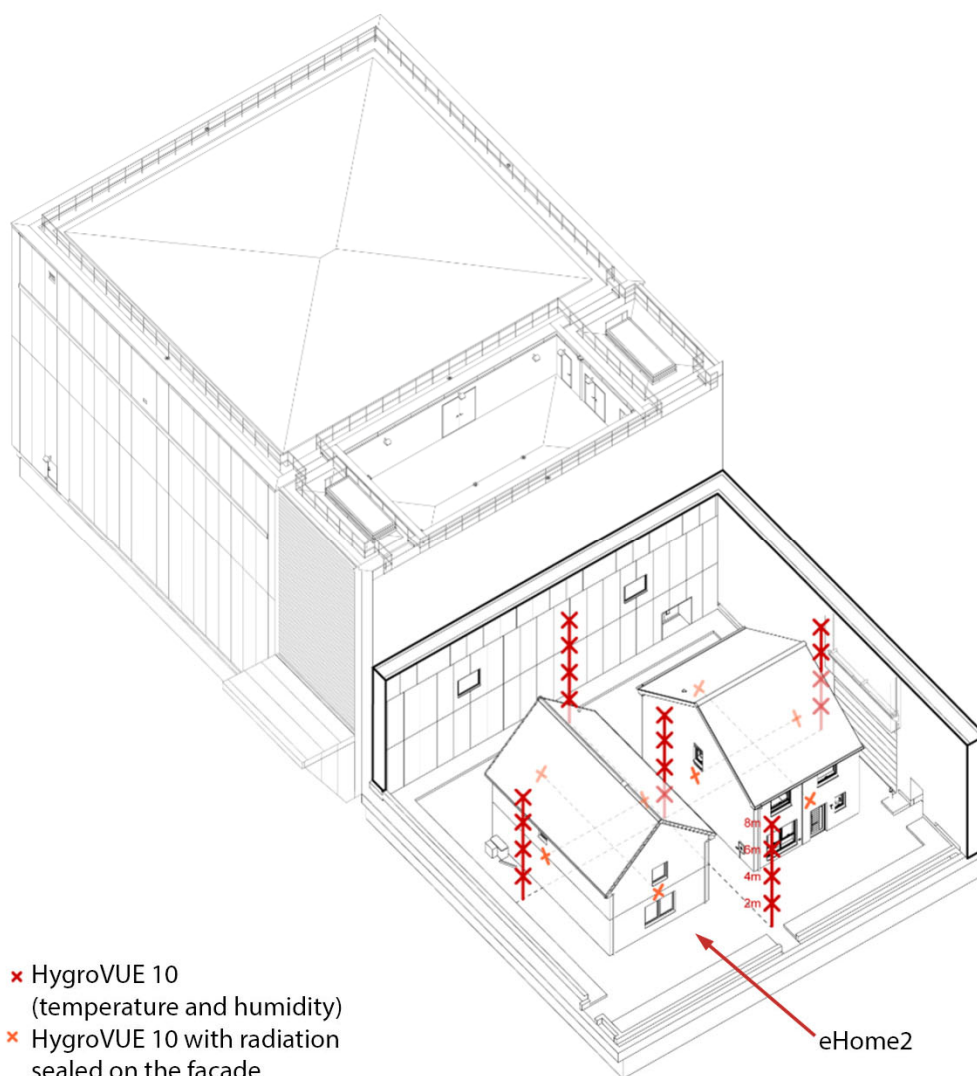
eHome2

Figure 5. Diagram of air temperature and humidity sensor locations within the chambers.

The following variables were monitored at one-minute time intervals in eHome2: air temperature in seven points in each room; operative temperature in seven points in each room; relative humidity in the geometric center of each room; electrical energy consumption; heat meter output on ASHP primary flow and return; and electrical energy consumption by circuit and by individual power outlet. Whole house sensor locations and heat emitters in eHome2 are shown in Figure 6.
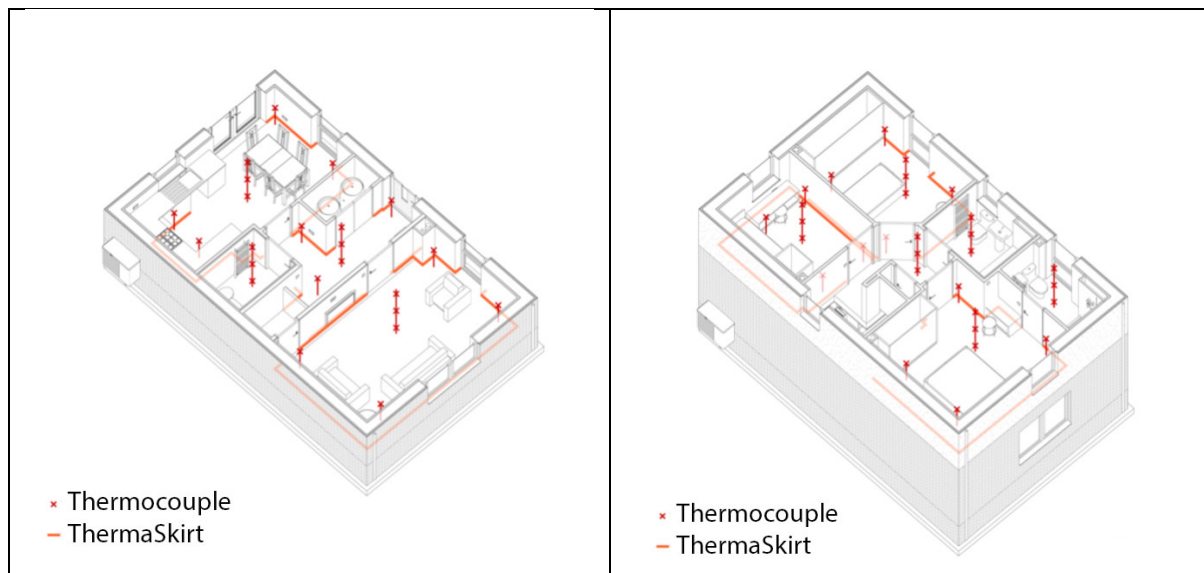
Figure 6. Heating emitters and thermocouples in eHome2 downstairs (**left**) and upstairs (**right**).

The rationale for the choice of the sensor locations in Figures 5 and 6 was to capture the volume distribution and volume stratification of the measurements in the Chamber and in each room of eHome2.

The experiments reported in this article are based on measurements obtained using the equipment listed in Table 4. Measurements were recorded at one-minute intervals by the Energy House 2.0 monitoring system.

Table 4. Measurement equipment used in eHome2 heating system tests.

Measurement	Equipment	Uncertainty
ASHP energy and power output	Sharkey 775 heat meter (Diehl Metering, Halifax, UK)	±1 %
ASHP flow rate	Sharkey 775 ultrasonic flow meter (Diehl Metering, Halifax, UK)	±1 %
ASHP flow and return temperature	PT-100 RTD (Sterling Sensors, Oldham, UK)	±0.3 °C
Internal shielded air temperature	Type-T thermocouples (calibrated to ± 0.1 °C) (RS Components, Corby, UK)	±0.1 °C
Mid-room shielded air temperatures	Campbell Scientific HygroVUE10 (20 to 60 °C) (Campbell Scientific, Shepshed, UK) [30]	±0.1 °C
Chamber air temperatures	Campbell Scientific HygroVUE10 (−40 to 70 °C) (Campbell Scientific, Shepshed, UK) [30]	±0.2 °C
Element surface temperatures	Type-T thermocouples (calibrated to ± 0.1 °C) (RS Components, Corby, UK)	±0.1 °C
Relative humidity	Campbell Scientific HygroVUE10 (Campbell Scientific, Shepshed, UK) [30]	±1.5 %
Black globe temperature	Type-T thermocouple in 40 mm diameter globe (RS Components, Corby, UK)	±0.1 °C

2.5. Machine Learning of the HTC Using Measured Data

Machine learning of the HTC was carried out using the whole house temperature, the chamber temperature, and the heat input from the heating system. As there were 53 temperatures measured in the house, a simplified whole house temperature was calculated as follows:

$$T_r = \frac{\sum_{i=1}^{i=10} T_i \times A_i}{\sum_{i=1}^{i=10} A_i} \tag{20}$$

where

T_i—middle shielded room temperature for each individual zone (°C);
A_i—floor area of each individual zone (m²);
i—individual zone index as in Table 5.

Table 5. eHome2 floor areas (source [28]).

	Individual Zone Index i	Zone	Floor Area (m²)
	1	Living Room	17.17
	2	Hall	7.81
Ground Floor	3	Kitchen + Dining	7.77 + 6.35
	4	WC	2.79
	-	Store 1	1.68
	5	Bedroom 1	12.29
	6	Bedroom 2	9.86
	7	Bedroom 3	7.51
First Floor	8	Landing	6.09
	9	Bathroom	3.89
	10	En-suite	3.19
	-	Store 2	0.44

The machine learning of the HTC is based on the following rearranged Equation (15):

$$T_r = T_{r,0} + (T_a - T_{r,0} + \frac{Q_{int} + Q_{sol}}{HTC}) \times (1 - e^{-\frac{t}{tc}}) \tag{21}$$

As internal heat input Q_{int}, solar input Q_{sol}, and the outdoor–indoor temperature difference can influence the building slightly differently in comparison with their measured values, the measurement scaling factors w_1, w_2, and w_3 are introduced into Equation (21) as follows:

$$T_r = T_{r,0} + ((T_a - T_{r,0}) \times w_1 + \frac{Q_{int} \times w_2}{HTC} + \frac{Q_{sol} \times w_3}{HTC}) \times (1 - e^{-\frac{t}{tc}}) \tag{22}$$

In this case, Q_{sol} was set to zero, to correspond to the controlled conditions in the Energy House 2.0 Environmental Chamber 1.

The machine learning of the HTC is based on setting up a fitness function as a root mean squared error between the internal room temperature calculated using Equation (22) and the measured internal room temperature calculated using Equation (20). The genetic algorithm was then used to evolve the values of HTC, tc, w_1, w_2, and w_3 to minimize the fitness function. This is performed on a day-by-day basis, using the measured values recorded at one-minute intervals and averaged to ten-minute intervals prior to starting the learning process.

As can be seen from Figure 7, the learning is based on the minimization of errors between calculated and monitored room-air temperature. Minimization of errors can be achieved using several different algorithms: the Newton–Raphson method, bracketing of

minimum, simulated annealing, downhill simplex method, steepest descent method, and others [31]. However, most of these methods start the search for a minimum from a single point of a solution space and are often locked into a local minimum. As Equation (22) shows, our solution space is five-dimensional, so the probability of locking into a local minimum when starting the search from a single point of the solution space is high. Therefore, a minimization algorithm that starts from multiple points of the solution space is preferable, and genetic algorithms have that capability. As several simulation tools, including DesignBuilder [18] and JEPus [32], use A fast and elitist multiobjective genetic algorithm: NSGA-II [33] for optimization, including minimization, the NSGA-II algorithm was considered for this research. However, as implementing NSGA-II proved to be time-consuming, a bespoke genetic algorithm was developed.
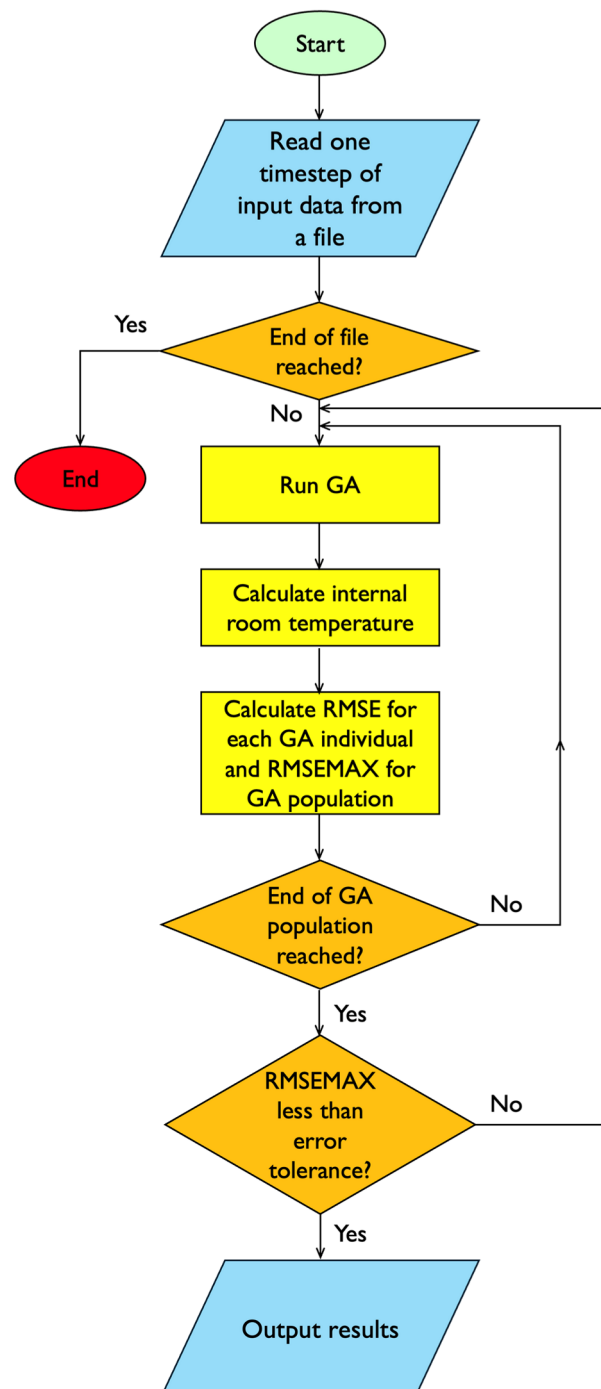
Figure 7. A flowchart summary of the main steps of the machine learning process.

The chosen GA population size was 100 chromosomes, each combined from the five unknown parameters in Equation (22). The GA parameters were experimented with between a 20% and 80% crossover rate and up to a 10% mutation rate and the convergence criterion was set to achieve RMSEMAX less than a chosen error tolerance. The error tolerance had to be adjusted based on the quality of data, between 1.7 °C and 0.5 °C, as explained in the Discussion section.

The machine learning was implemented as a bespoke algorithm in Java programming language, where the input data stream consisted of monitored data and the output data stream consisted of the HTC and the RMSE. The elapsed time for processing of 140 days of data at ten-minute timesteps lasted 0.23 s and of 12 days of data at ten-minute timesteps lasted 0.13 s on an Apple MacBook Pro with Apple M3 Max processor.

3. Experiments and Results

The variability in the HTC will now be investigated in two steps. First, the variability during a dynamic heating and cooling down test will be investigated using a calibrated simulation model of eHome2. Second, the HTC will be calculated from an input data stream from a fully instrumented and monitored eHome2 under controlled conditions in Energy House 2.0 Environmental Chamber 1, containing internal and external air temperatures and heat input at ten-minute time steps.

3.1. HTC During a Dynamic Heating and Cooling-Down Test Simulation with a Calibrated Model

Let us first consider the changes of the HTC during a simulation of eHome2 using a calibrated EnergyPlus model introduced in Section 2.4. During the heating phase, the result of internal temperature change occurs as a consequence of a constant heat input of 3.5 kW between hours 24 and 168. After that time period, the heating is switched off and the building cools down until reaching the equilibrium by the hour 360.

As the HTC = Q/ΔT, where Q is a constant heat input, and ΔT is the temperature difference between internal and external air temperatures, the HTC changes as follows:

$$t(24) \leq HTC = Q \times f(1/\Delta T) \leq t(168) \tag{23}$$

$$HTC = 0 \geq t(169) \tag{24}$$

where the HTC is a function of 1/ΔT in Equation (23) and t(x) denotes time in hours.

As can be seen from Figure 8, the HTC is greater than 1000 W/K at time t = 24 h when the test starts, and it goes to a value of 86.7 W/K when steady state is reached at time t = 168 h. Subsequently, it drops down to the HTC = 0 at time t = 169, when heating is switched off and the internal temperature is in a free fall from the maximum temperature of T = 45 °C at time t = 168 h, down to 5 °C at time t = 360 h. The time constant remains constant between heating and cooling at the value of 36.5 h.
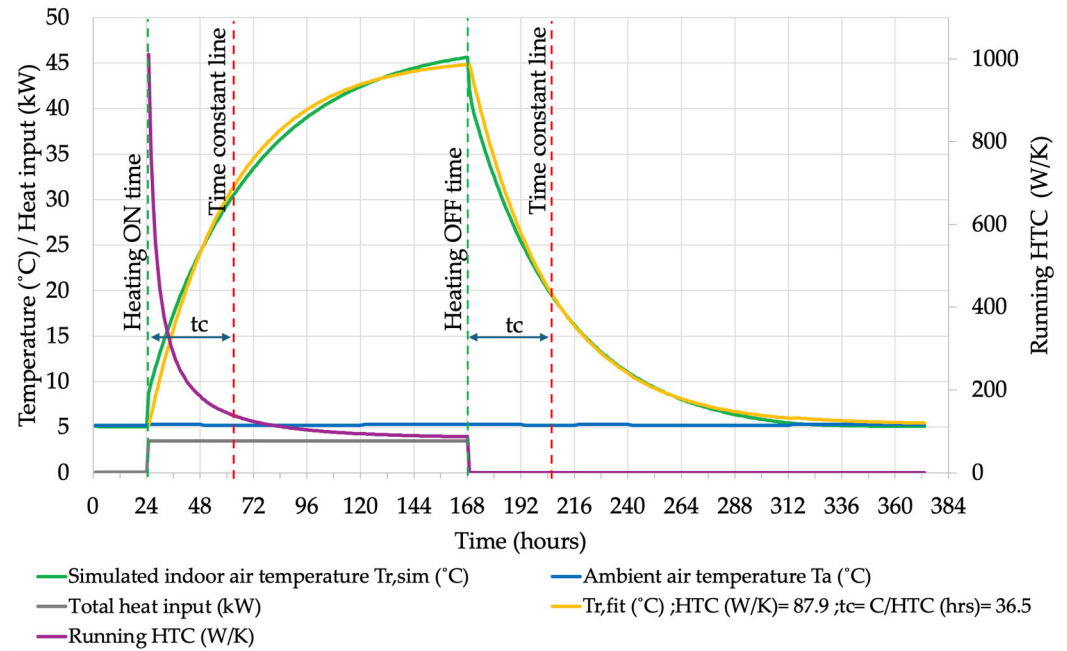
Figure 8. Results of the dynamic heating and cooling simulation.

The simulation results in Figure 8 were subjected to curve-fitting, where the heated part was modelled with Equation (25) and the cooling-down part was modelled with Equation (26):

$$T_{r,fit} = T_a + (T_{r,max} - T_a) \times (1 - e^{-\frac{t}{tc}}) \tag{25}$$

$$T_{r,fit} = T_a + (T_{r,max} - T_a) \times (e^{-\frac{t}{tc}}) \tag{26}$$

where

$T_{r,fit}$—room air temperature curve-fitted to simulation temperature $T_{r,sim}$ (°C);

T_a—ambient air temperature kept constant throughout the simulation in the environmental chamber (°C);

$T_{r,max}$—maximum room temperature achieved during the simulation

tc—time constant

t—time (hours).

The root mean squared error between the simulated and fitted internal room-air temperature shown in Figure 8 was as follows:

$$RMSE = \sqrt{\frac{\sum_1^N (T_{r,sim} - T_{r,fit})^2}{N}} = 0.93 \, °C \tag{27}$$

where N = 349 was the total number of hours of the simulation.

This means that the time constant, the temperature differences between room air temperature and ambient air temperature, and the time were sufficient for an accurate simplified model of a dynamic heat transfer in a building. It also means that the HTC depends on the temperature difference between internal and external air temperatures.

As shown in Equation (18), the time constant is inversely proportional to thermal diffusivity, and hence the curve-fitted model of the simulation in Equations (25)–(26) is based on thermal diffusivity as a fundamental building physics property. Therefore, models based on the time constant are effectively based on thermal diffusivity.

The results in this section represent the first step in creating experimental evidence of the HTC variability.

3.2. Machine Learning of Daily HTC Variations Using Measured Data

The data used for this analysis were monitored in one-minute intervals and averaged to ten-minute intervals, as shown in Figure 9. The first set of results obtained is shown in Figure 10, based on Equation (22) and using a genetic algorithm (GA) to evolve the building physics parameters while minimizing the RMSE fitness function.
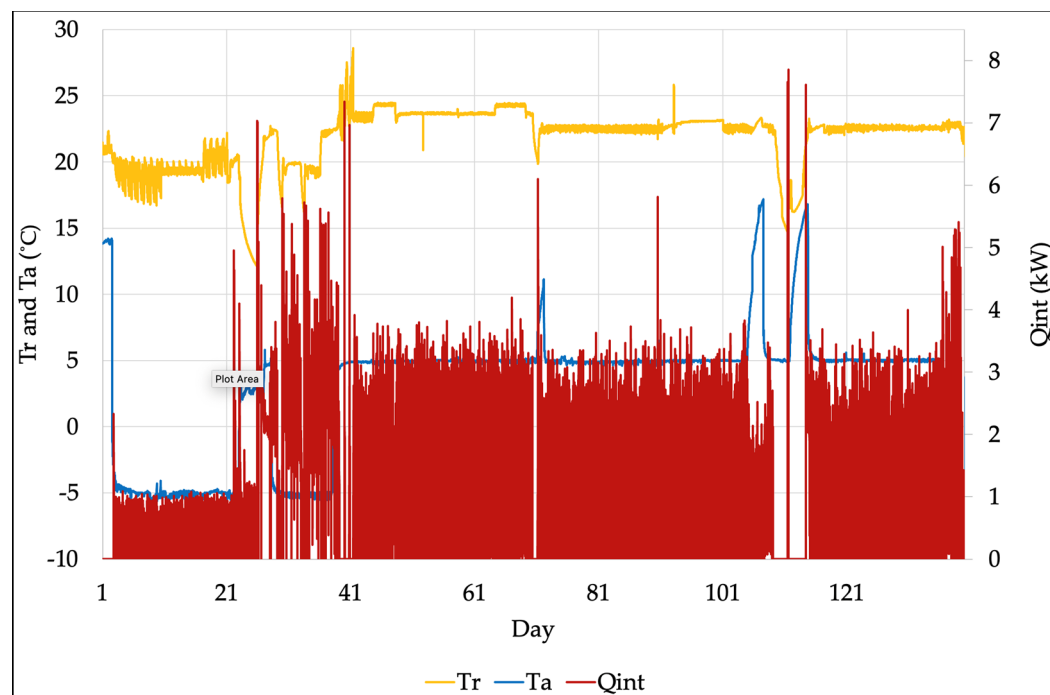
Figure 9. Source data for machine learning over 140 days.
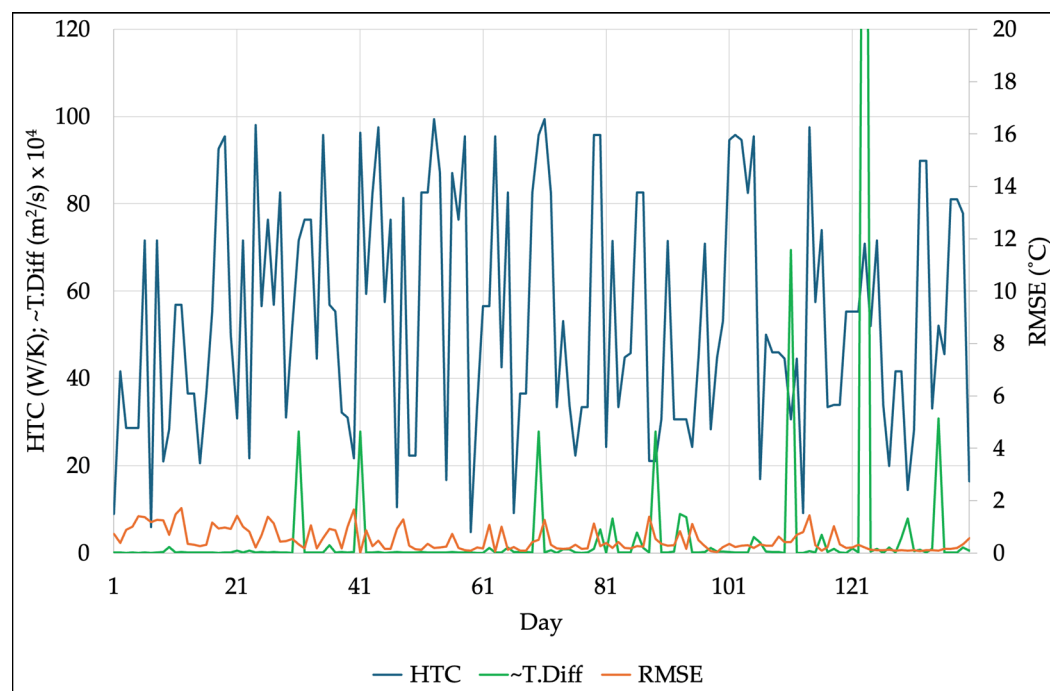
Figure 10. HTC obtained through machine learning from measured data over a period of 140 days in 2024.

As can be seen from this figure, the HTC varies for each day over 140 days of a data set recorded in 2024, with RMSE reaching 1.7 °C. This was achieved while the error

tolerance for GA learning was set to RMSEMAX >= 2.0 °C. The error tolerance is used to force the GA algorithm to go into recursive learning until RMSEMAX becomes lower than the set value.

Could the reason for the magnitude of RMSE of 1.7 °C be caused by the data used? To investigate this, a new error tolerance of 1.2 °C was set on the same data set and the learning time became exceptionally long, so the process was terminated manually. In order to investigate lower error tolerances, a much shorter and cleaned-up data set of 12 days was selected from 2023 (Figure 11), and the GA learning was rerun, giving the results in Figure 12.
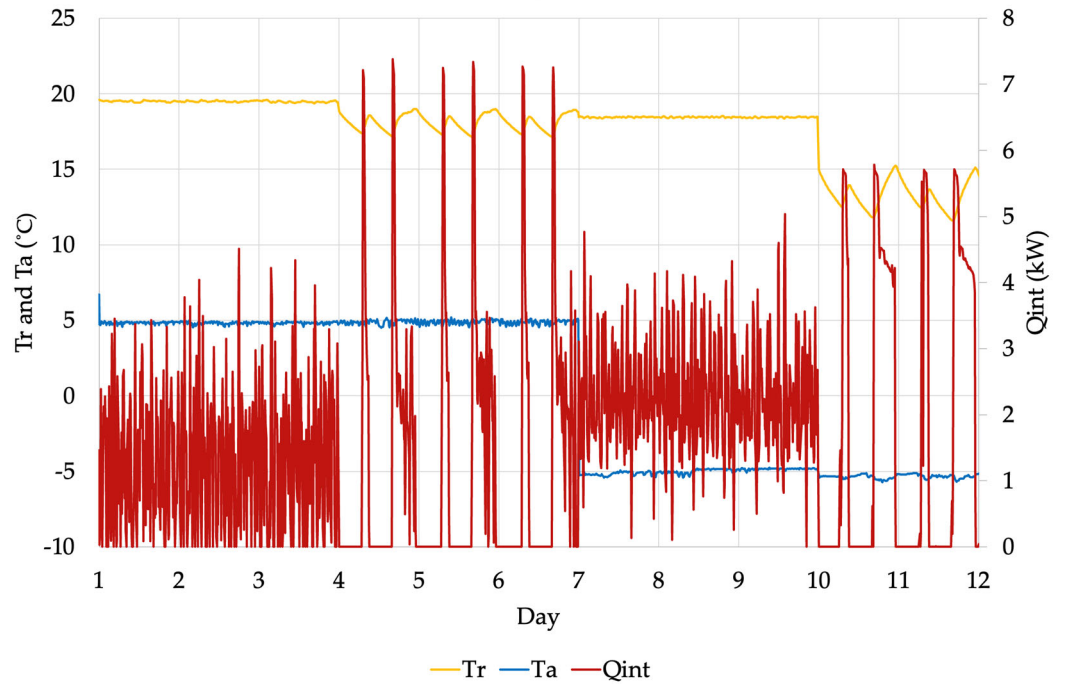
Figure 11. Source data for machine learning over 12 days.
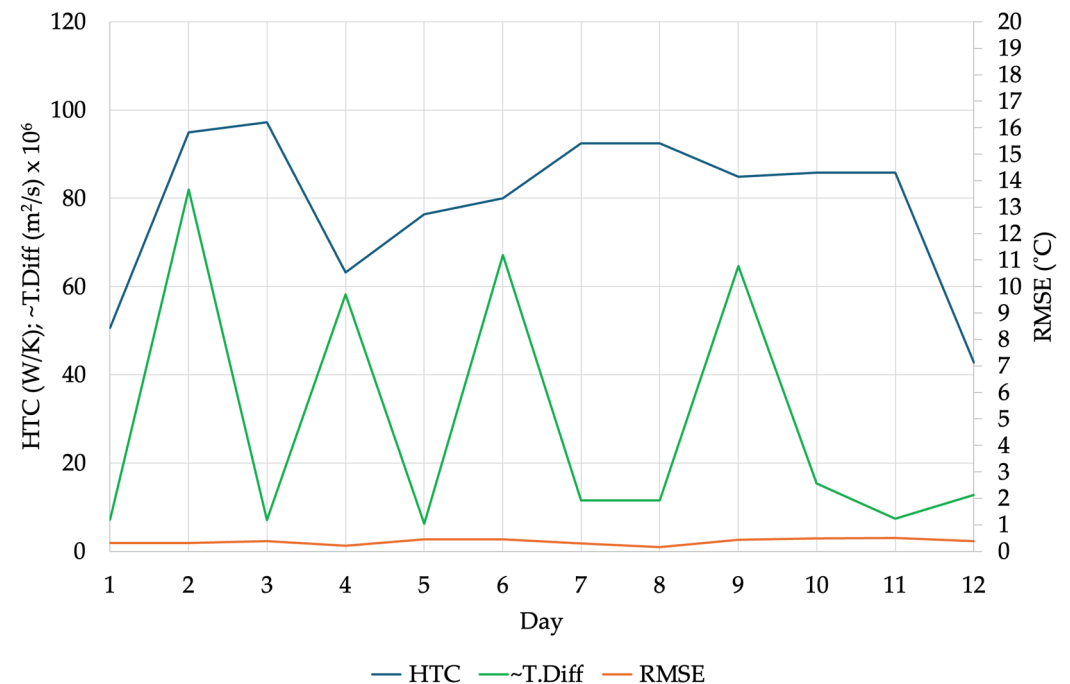
Figure 12. HTC obtained through machine learning from measured data over a period of 12 days in 2023.

As can be seen from this figure, the RMSE does not exceed 0.5 °C in the shorter and cleaned-up data set. Therefore, a better quality of data will increase the accuracy of results.

The results in Figures 10 and 12 show that the HTC depends on the temperature differences between internal and external air temperatures and the heat input, as shown in Figures 9 and 11, and that the accuracy of its calculation depends on the quality of data—the better the data, the lower the RMSE.

Figures 10 and 12 also show thermal diffusivity variation, as derived from Equation (18). As shown in Equation (11), thermal diffusivity is a ratio between thermal conductivity and density-specific heat product. Considering that the HTC is proportional to thermal conductivity, it can be expected that the time series representing the HTC and thermal diffusivity would go in the same direction in these two figures. However, these time series are a daily representation of both parameters. Considering that the heat transfer dynamics occur much deeper at the ten-minute timestep corresponding to the source data, the effects of the dynamic relationship between the HTC and thermal diffusivity do not seem to be correlated at this much longer daily representation.

As the HTC does not appear to be constant, using a constant value as an indicator of building energy performance will lead to a performance gap between the as-designed and as-built performance.

The results in this section represent the second step in creating the experimental evidence of the HTC variability.

4. Discussion

The previous section presented the evidence of variability in the HTC using dynamic heating and cooling performance analysis of a calibrated simulation model, as well as using machine learning of the HTC from measured building performance data over longer and shorter data sets. The HTC variation in the results from Figure 10 is in the range between 0 W/K and 99.7 W/K and in the results from Figure 12, the HTC is in the range between 42.7 W/K and 97.2 W/K. These results are significantly more variable than the HTC results in Table 1 obtained as constants under specific test conditions and with variations due to measurement uncertainties. As can be seen from that table, the co-heating test result was 76.7 W/K and the error tolerance was ±2.1 W/K. The QUB test result was 65.1 W/K and the error tolerance was ±5.6 W/K, while the test differed from the co-heating test by −15%. The Veritherm test result was 71.9 W/K, and it differed from the co-heating test by −6%. Therefore, the tests that seek the HTC as a constant value already produce different results and with different discrepancies between the different test methods. Our results, which reveal the underlying dynamics of the HTC, can be used to put the variations in constant HTCs into context: in essence, the HTC is a variable, and different methods that seek its value as a constant will inevitably produce different results.

But where does this HTC dynamic variability come from? While the HTC is widely considered to be of a constant value measured by different methods when reaching steady state, building heat transfer is highly dynamic and the steady state practically never occurs except in artificially created test conditions. The HTC represents a coefficient of heat transfer that occurs as result of thermal resistance of the building envelope, its inertia to lose or gain heat. That heat transfer slowdown is caused by thermal insulation, and by air tightness that works in the same direction as thermal insulation, as well as thermal diffusivity that effects the dynamics of heat transfer. Considering these heat transfer mechanisms, it becomes clearer that the HTC is not constant and cannot be constant.

Section 3.1 demonstrates that the HTC falls to zero when heat input is switched off and the building temperature is in a free fall , and therefore using a constant non-zero value of the HTC will lead to discrepancies between as-designed and as-built buildings.

The root mean squared error in Figure 10 shows variability of up to 1.7 °C. The RMSE magnitude could be caused by a few gaps in the monitored data revealed during data preparation for this analysis. These gaps occurred due to timing issues in the recording of data, so that some temperatures in Equation (20) were not available for all time steps. In such cases, all the temperatures from the timesteps where some temperatures were missing were deleted, and the resultant gap was then eliminated by stitching up the data before and after the gap.

This process is illustrated in Figure 13, where the red, dotted line shows that some data are missing for the corresponding timestep. This typically occurred at the end of some months. In such cases, the data below the red dotted line were deleted, and data from the start of the next month were appended (stitched up). This process appears to have introduced minor step changes in the data, thus increasing the RMSE in the instances where the stitching up occurred.

Figure 13. Illustration of dealing with data gaps.

As a result of cleaning up the data, the root mean squared error in Figure 12 was much improved, with a maximum of 0.5 °C. In this much shorter data set, all temperatures and other parameters were carefully aligned for each timestep, so that no gaps occurred and no data stitching up was required.

However, in both cases, the root mean squared error is greater than zero. This can be due to a daily calculation of the HTC where dynamics of heat transfer throughout 24 h has been represented with a single number.

The comparison between the results in Figures 10 and 12 clearly demonstrate uncertainties related to experimental measurements. In the example from Figure 10, data contained spikes that occurred as result of eliminating the gaps as illustrated in Figure 13, and for that reason, the learning process error tolerance had to be increased to 2.0 °C to enable the learning to be completed in a timely manner. With cleaner data in Figure 12, it was possible to reduce the error tolerance to 0.5 °C without a detrimental effect on the learning completion time. This analysis has therefore revealed the importance of data integrity in the machine learning process.

This analysis has also revealed some limitations in our model and methodology. We explained earlier that the genetic algorithm approach was chosen as it was capable of searching the solution space from multiple starting points (Figure 14b), in preference to other methods that search the solution space from a single starting point (Figure 14a).

| (**a**) Search from a single starting point | (**b**) Search from multiple starting points |
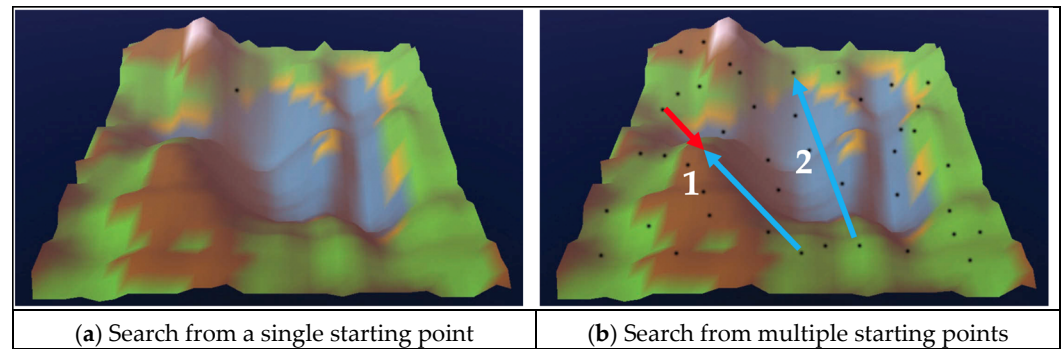
Figure 14. Conceptual representation of a multi-dimensional solution space. (1 represents a crossover destination, and the blue and red arrow represent the chromosome origins from different parents; 2 represents a mutation destination, and the blue arrow represents the chromosome origin from a single parent).

This is important, because the search from a single starting point can easily lock into a local minimum, rather than a global minimum, and thus produce a sub-optimum solution. In the case of the genetic algorithm, the search from multiple starting points uses a crossover (labelled as 1 in Figure 14b where the blue and red arrow represent the chromosome origins from different parents) and a mutation (labelled as 2 in the same figure, where the blue arrow represents the chromosome origin from a single parent). The crossover will produce an offspring that will be placed along line 1 between the two parents, and the mutation will create an offspring in a totally new part of the solution space, indicated by line 2 . Despite the thorough coverage of the solutions space, we can never be sure that a global optimum will be reached. This is evident from the sensitivity of the learning process to the error tolerance discussed earlier. With a more relaxed error tolerance the learning process is faster, but this also means that it spends less time looking for the global minimum and has a greater chance of locking into a local minimum, therefore a sub-optimum. We will investigate this further in our future research.

The results in Section 3.2 demonstrate a "reverse-engineering" of the HTC from an ongoing monitoring of a building, without any preconditioning or other preparations of the building.

5. Conclusions

The heat transfer coefficient (HTC), a standard indicator of building energy performance, is assumed by the industry to be a constant value with a limited variability due to test conditions, measurement methods, and measurement errors. However, the experimental evidence from this research shows that the HTC is dynamically variable.

The HTC quantifies the thermal resistance of a building envelope and its inertia to losing or gaining heat. This heat transfer slowdown is achieved through thermal insulation, airtightness that aligns with the direction of thermal insulation, and thermal diffusivity, which forms the foundation of dynamic heat transfer. Considering these heat transfer mechanisms, it becomes evident that the HTC is not a constant and generally it cannot be maintained as such. This variability challenges the traditional use of the HTC in building performance analysis and calls for a re-evaluation of its application.

The approach introduced in this article has demonstrated automated learning of the HTC by reading monitored data into a bespoke genetic algorithm developed in Java programming language. Effectively, the HTC was "reverse-engineered" from data from an ongoing monitoring of a building, without any preconditioning or other preparations of that building.

Although this research used experimental data recorded at one-minute intervals and averaged to ten-minute intervals, the gaps in the data caused long learning times. It was therefore decided to increase the error tolerances to enable timely completion of the learning process. This is believed to have caused RMSE errors of up to 1.7 °C. These errors were subsequently reduced to 0.5 °C in a shorter, cleaned-up data set. However, the errors remained above zero, most likely because of the daily calculation of the HTC, representing a coarse approximation of the underlying daily dynamics.

The future research will focus on reducing the RMSE from machine learning of the HTC on a day-by-day basis by using a higher resolution sub-daily approach, as well as a further cleaning of the input data sets and reducing error tolerances. This approach will undergo further application to different building topologies and climate scenarios to investigate its applicability in different contexts. We will also be investigating implementation pathways for integrating OHTC into building energy standards, working with our partners from IEA EBC—Annex 94—Validation and Verification of In situ Building Energy Performance Measurement Techniques [34].

Does the evidence of dynamic variability in the HTC mean that the measurement of the HTC as a constant has been fundamentally flawed? The findings presented in this article do not undermine the value of the established methods for measuring the HTC as a constant, especially for comparing buildings under steady-state conditions on a level playing field . Instead, we propose distinguishing between two types of HTCs: the constant value, which can be referred to as a test or theoretical HTC (THTC), and the dynamically variable value introduced in this article, which can be referred to as an operational HTC (OHTC).

The THTC remains useful for standardized comparisons across buildings under controlled conditions. In contrast, the OHTC provides new insights into real-world building performance by reflecting dynamic conditions. It is important to note, however, that relying solely on the THTC for evaluating annual building performance will result in a performance gap between the designed and actual performance.

So, is the HTC a constant with limited variability, or is it dynamically variable? In practice, it is both—depending on the measurement context and the intended use. When measured under controlled, standardized conditions, the HTC serves as a constant (THTC). When derived from real-time monitored data using machine learning under naturally varying conditions, it becomes dynamically variable (OHTC).

Considering the limitations in the THTC and the variability in the OHTC, the key recommendation to practitioners and research community arising from this research is to use dynamic modelling and simulation for building performance assessment routinely instead of relying purely on steady-state parameters.

Nomenclature

ρ	density (kg/m³)
A_i	floor area of each individual zone (m²)
A_i	surface area of the i-th building element (m²)
B	proportionality constant in Equation (18)
C	effective thermal capacitance in MJ/K
c	specific heat (J/(kg·K))
d	wall thickness in meters (m)
GA	Genetic Algorithm
H_c	conductive heat loss coefficient (W/K)
H_{tb}	thermal bridging heat loss coefficient (W/K)
HTC	heat transfer coefficient (W/K)
H_v	ventilation and infiltration heat loss coefficient (W/K)
i	individual zone index as in Table 5
k	thermal conductivity in W/(m·K)
L_i	length of the i-th linear thermal bridge (m)
m	mass (kg)
n	number of building elements
N	volume air change per hour (h⁻¹)
OHTC	operational HTC (W/K)
$\dot{q}$	heat flux (W/m²)
Q	overall heat loss rate (W)
Q_{int}	internal heat gain in the building arising from heating or from casual gains (W).
Q_{loss}	heat gain from solar radiation (W)
Q_{sol}	heat gain from solar radiation (W)
$R_1, R_2, R_3\ldots$	resistances of individual construction layers (m²K/W)
R_i	internal surface resistance (m²K/W)
RC model	Resistance-Capacitance model
RMSE	root mean squared error (°C)
RMSEMAX	maximum RMSE over entire GA population (°C)
R_o	external surface resistance (m²K/W)
T	temperature (°C)
t	time (s)
T_{amb}	difference between ambient air temperature and the initial room temperature $T_a - T_{r,0}$. (°C)
~T.Diff	proportional to thermal diffusivity.
THTC	test or theoretical HTC (W/K)
T_i	internal air temperature (K)
T_i	middle, shielded room temperature for each individual zone (°C)
T_o	external air temperature (°C).
T_{room}	difference between room temperature and the initial room temperature $T_r - T_{r,0}$ (°C)
OTTV	overall thermal transfer value (W/m²)
QUB	quick U-value of buildings
U_i	thermal conductance of the i-th building element (W/(m²K))
V	volume (m³)
z	proportionality constant that represents the relationship B/V in Equation (19).
α	thermal diffusivity (m²/s)
Ψ_i	linear thermal transmittance of the i-th thermal bridge (W/(m·K))

References

1.   *ISO 13789:2017*; Thermal Performance of Buildings—Transmission Heat Loss Coefficient—Calculation Method. ISO: Geneva, Switzerland, 2017.

2.   Fitton, R. *Building Energy Performance Assessment Based on In-Situ Measurements: Challenges and General Framework*; IEA EBC Annex 71; KU Leuven: Leuven, Belgium, 2021.

3.   Eastwood, M. Variability in the Heat Transfer Coefficient of Dwellings. Ph.D. Thesis, Loughborough University, Loughborough, UK, 2025. https://doi.org/10.26174/THESIS.LBORO.28381235.V1.

4.   Li, M. Thermal Performance of UK Dwellings: Assessment of Methods for Quantifying Whole-Dwelling Heat Loss in Occupied Homes. Ph.D. Thesis, Loughborough University, Loughborough, UK, 2022. https://doi.org/10.26174/THESIS.LBORO.19735699.V1.

5.   Sougkakis, V.; Meulemans, J.; Wood, C.; Gillott, M.; Cox, T. Field Testing of the QUB Method for Assessing the Thermal Performance of Dwellings: In Situ Measurements of the Heat Transfer Coefficient of a circa 1950s Detached House in UK. *Energy Build.* **2021**, *230*, 110540. https://doi.org/10.1016/j.enbuild.2020.110540.

6.   Ahmad, N.; Ghiaus, C.; Qureshi, M. Error Analysis of QUB Method in Non-Ideal Conditions during the Experiment. *Energies* **2020**, *13*, 3398. https://doi.org/10.3390/en13133398.

7.   Juricic, S.; Rabouille, M.; Challansonnex, A.; Jay, A.; Thébault, S.; Rouchier, S.; Bouchié, R. The Sereine Test: Advances towards Short and Reproducible Measurements of a Whole Building Heat Transfer Coefficient. *Energy Build.* **2023**, *299*, 113585. https://doi.org/10.1016/j.enbuild.2023.113585.

8.   Vighio, A.A.; Zakaria, R.; Ahmad, F.; Aminuddin, E. Real-Time Monitoring and Development of a Localized OTTV Equation for Building Energy Performance. *Civ. Eng. J.* **2025**, *11*, 544–564. https://doi.org/10.28991/CEJ-2025-011-02-09.

9.   Allinson, D. *Technical Evaluation of SMETER Technologies (TEST) Project*; Department for Business, Energy & Industrial Strategy: London, UK, 2022; p. 183.

10. Build Test Solutions & SOAP Retrofit. *SmartHTC Validation Report*; Build Test Solutions Ltd.: Northampton, UK, 2021.

11. Aico Utilising IOT Technology to Validate Retrofit Interventions (No. HomeLINK; p. 9) Available online: https://www.aico.co.uk/wp-content/uploads/2024/08/Retrofit-Validation-Case-Study-Aico-x-CorkSol.pdf (accessed on 30 March 2025).

12. Johnston, D.; Miles-Shenton, D.; Wingfield, J.; Farmer, D.; Bell, M. *Whole House Heat Loss Test Method (Coheating)*; Leeds Metropolitan University: Leeds, UK, 2012.

13. *BS EN 17887-1:2024*; Thermal Performance of Buildings. In Situ Testing of Completed Buildings. Data Collection for Aggregate Heat Loss Test (Part 1). British Standards Institution: London, UK, 2024.

14. Marshall, A.; Fitton, R.; Swan, W.; Farmer, D.; Johnston, D.; Benjaber, M.; Ji, Y. Domestic Building Fabric Performance: Closing the Gap between the in Situ Measured and Modelled Performance. *Energy Build.* **2017**, *150*, 307–317. https://doi.org/10.1016/j.enbuild.2017.06.028.

15. Farmer, D.; Gorse, C.; Swan, W.; Fitton, R.; Brooke-Peat, M.; Miles-Shenton, D.; Johnston, D. Measuring Thermal Performance in Steady-State Conditions at Each Stage of a Full Fabric Retrofit to a Solid Wall Dwelling. *Energy Build.* **2017**, *156*, 404–414. https://doi.org/10.1016/j.enbuild.2017.09.086.

16. Jack, R.; Loveday, D.; Allinson, D.; Lomas, K. First Evidence for the Reliability of Building Co-Heating Tests. *Build. Res. Inf.* **2018**, *46*, 383–401. https://doi.org/10.1080/09613218.2017.1299523.

17. HM Government BEIS. *SAP 10.2: The Government's Standard Assessment Procedure for Energy Rating of Dwellings*; BRE: Watford, UK, 2023.

18. DesignBuilder Software Ltd. *DesignBuilder*; DesignBuilder Software Ltd.: Stroud, UK, 2024.

19. Johnston, D.; Miles-Shenton, D.; Farmer, D. Quantifying the Domestic Building Fabric Performance Gap . *Build. Serv. Eng. Res. Technol.* **2015**, *36*, 614–627. https://doi.org/10.1177/0143624415570344.

20. Parker, J.; Farmer, D.; Johnston, D.; Fletcher, M.; Thomas, F.; Gorse, C.; Stenlund, S. Measuring and Modelling Retrofit Fabric Performance in Solid Wall Conjoined Dwellings. *Energy Build.* **2019**, *185*, 49–65. https://doi.org/10.1016/j.enbuild.2018.12.010.

21. Fitton, R.; Diaz Hernandez, H.; Farmer, D.; Henshaw, G.; Sitmalidis, A.; Swan, W. *Saint Gobain & Barratt Developments "eHome2" Baseline Performance Report*; ERDF & Innovate UK: Salford, UK, 2024.

22. Alzetto, F.; Pandraud, G.; Fitton, R.; Heusler, I.; Sinnesbichler, H. QUB: A Fast Dynamic Method for in-Situ Measurement of the Whole Building Heat Loss. *Energy Build.* **2018**, *174*, 124–133. https://doi.org/10.1016/j.enbuild.2018.06.002.

23. Energy Systems Catapult. *Veritherm: Identifying Consumer Routes to Market for Thermal Testing*; Energy Systems Catapult: Birmingham, UK, 2024.

24. Jankovic, L. *Designing Zero Carbon Buildings: Embodied and Operational Emissions in Achieving True Zero*, 3rd ed.; Routledge/Taylor & Francis Group: Oxford, UK; New York, NY, USA, 2024; ISBN 978-1-03-237871-8.

25. BRE Group Standard Assessment Procedure SAP 10. Available online: https://bregroup.com/expertise/energy/sap/sap10 (accessed on 28 March 2025).

26. Lienhard, J.H.V.; Lienhard, J.H.I.V. *A Heat Transfer Textbook*, 6th ed.; Phlogiston Press: Cambridge, MA, USA, 2024.

27. Fourier, J.B.J. *The Analytical Theory of Heat*, 1st ed.; Cambridge University Press: Cambridge, UK, 2009; ISBN 978-1-108-00178-6.

28. Tsang, C.; Fitton, R.; Zhang, X.; Henshaw, G.; Diaz Hernandez, H.; Farmer, D.; Allinson, D.; Sitmalidis, A.; Dgali, M.; Jankovic, L.; et al. *Dataset for Article: "Calibration of Building Performance Simulations for Zero Carbon Ready Homes: Two Open Access Case Studies in Controlled Conditions"*; University of Salford: Manchester, UK, 2025.

29. Department of Energy. *DOE EnergyPlus*; Department of Energy: Washington, DC, USA, 2024.

30. HygroVUE10—Digital Temperature and Relative Humidity Sensor with M12 Connector. Available online: https://www.campbellsci.com/hygrovue10 (accessed on 4 July 2023).

31. Press, W.H. (Ed.) *Numerical Recipes: The Art of Scientific Computing*, 3rd ed.; Cambridge University Press: Cambridge, UK; New York, NY, USA, 2007; ISBN 978-0-521-88068-8.

32. Zhang, Y. JEPlus—A Parametric Tool for EnergyPlus and TRNSYS. 2020. Available online: https://www.jeplus.org/wiki/doku.php (accessed on 30 March 2025).

33. Deb, K.; Pratap, A.; Agarwal, S.; Meyarivan, T. A Fast and Elitist Multiobjective Genetic Algorithm: NSGA-II. *IEEE Trans. Evol. Comput.* **2002**, *6*, 182–197. https://doi.org/10.1109/4235.996017.

34. IEA EBC About ǀǀ IEA EBC ǀǀ Annex 94. Available online: https://annex94.iea-ebc.org/about (accessed on 30 March 2025).